Journal of Marine Science and Application (2019) 18:153–159
https://doi.org/10.1007/s11804-019-00076-8

RESEARCH ARTICLE

Analysis of the Hydrodynamic Performance of an Oyster Wave Energy Converter Using Star-CCM+

Zheng Yuan[1] · Liang Zhang[1] · Binzhen Zhou[1] · Peng Jin[1] · Xiongbo Zheng[2]

Received: 12 October 2017 / Accepted: 3 August 2018 / Published online: 4 March 2019

Abstract
A two-dimensional numerical Computational Fluid Dynamics (CFD) model is established on the basis of viscous CFD theory to investigate the motion response and power absorption performance of a bottom-hinged flap-type wave energy converter (WEC) under regular wave conditions. The convergence study of mesh size and time step is performed to ensure that wave height and motion response are sufficiently accurate. Wave height results reveal that the attenuation of wave height along the wave tank is less than 5% only if the suitable mesh size and time step are selected. The model proposed in this work is verified against published experimental and numerical models. The effects of mechanical damping, wave height, wave frequency, and water depth on the motion response, power generation, and energy conversion efficiency of the flap-type WEC are investigated. The selection of the appropriate mechanical damping of the WEC is crucial for the optimal extraction of wave power. The optimal mechanical damping can be readily predicted by using potential flow theory. It can then be verified by applying CFD numerical results. In addition, the motion response and the energy conversion efficiency of the WEC decrease as the incident wave height increases because the strengthened nonlinear effect of waves intensifies energy loss. Moreover, the energy conversion efficiency of the WEC decreases with increasing water depth and remains constant as the water depth reaches a critical value. Therefore, the selection of the optimal parameters during the design process is necessary to ensure that the WEC exhibits the maximum energy conversion efficiency.

Keywords Wave energy converter · Oyster · Energy conversion efficiency · Optimum PTO damping · Nonlinear regular wave

1 Introduction

Traditional energy sources have dwindled and environmental pollution and climate warming problems caused by the use of fossil fuels have intensified with the rapid growth of global energy demands; thus, renewable energy is attracting growing attention (Kerr 2007). Wave energy, which has high power density and extensive distribution, is an inexhaustible renewable clean energy source. In recent years, many countries, such as the UK, the USA, Norway, Australia, Ireland, and Denmark, have contributed to the rapid development of wave energy by massively investing in research on wave energy devices. Wave energy conversion technology, however, remains uncommercialized. Raft, point absorber (Ning et al. 2016a, 2017; Chen et al. 2018a,b,c), oscillating water column (He et al. 2012; Ning et al. 2016b), and flap types (Sun et al. 2018) are the main forms of wave energy devices. The flap wave energy converter (WEC) can be categorized as gravity and bottom-hinged flaps in accordance with hinge position (Salter 1974). Bottom-hinged flaps have numerous advantages, such as a broad frequency response range, adaptability under extreme loads, high efficiency under conventional sea conditions, simple structure, easy installation and maintenance, and low cost.

Article Highlights
- The energy conversion efficiency of the flap-type WEC decreases as incident wave height increases because of energy loss.
- The energy conversion efficiency of the flap-type WEC decreases as water depth increases.
- The maximum energy conversion efficiency is achieved when the optimal PTO damping calculated with the linear frequency domain theory is selected.

✉ Binzhen Zhou
zhoubinzhen@hrbeu.edu.cn

[1] College of Shipbuilding Engineering, Harbin Engineering University, Harbin 150001, China

[2] College of Science, Harbin Engineering University, Harbin 150001, China

It has been rapidly developed in recent years given its considerable application value in shallow offshore waters.

A large number of domestic and foreign works on the hydrodynamic performance of bottom-hinged flap wave energy have been performed by using different research methods, including analytical and numerical methods and physical model experiments. Folley et al. (2007a, b) analyzed the influence of parameter variation on the hydrodynamic performance of bottom-hinged flaps by applying a frequency domain model. They found that viscosity loss is proportional to the square of the swing speed of the flap under the assumptions of a single frequency linear wave, linear power take-off (PTO) damping, and small amplitude motion. Flocard and Finnigan (2010) analyzed the hydrodynamic performance of a cylindrical buoyant pendulum in a sink experiment with a scale ratio of 1/33 and different parameters, such as cylinder diameter, water depth, PTO damping, and moment of inertia. Adjusting the moment of inertia of the swing plate improved the conversion efficiency of the device. Chaplin and Aggidis (2007) analyzed the torque output of a buoyancy pendulum under extreme wave conditions in a tank test with a geometric scale of 1/100. Ogai et al. (2010) designed a suspension pendulum device that was installed before a coastal protective structure in a tank test. They then determined the influence of the device on the protective structure and the conversion efficiency of the device. Wei et al. (2015, 2016) investigated the influence of fluid viscosity on the dynamic performance of the bottom-hinged flap and compared CFD results with experimental results. Crooks et al. (2016) examined the nonlinear motion of a bottom-hinged flap at a large swing angle by comparing model test results and two numerical results. Henry et al. (2014) identified the mechanism underlying the effect of impact load on a bottom-hinged flap through impact tests. They compared their experimental results with two numerical results. By combining theoretical analysis, numerical simulation, and model experiments, Zhao et al. (2013) systematically evaluated the hydrodynamic performance of WECs. They emphasized the influence of PTO damping on the hydrodynamic performance of the device.

In this study, a two-dimensional bottom-hinged flap WEC under the condition of nonlinear regular waves is simulated on the basis of viscous CFD theory. The motion response and power absorption performance of the WEC are also analyzed. The accuracy of the numerical model is verified by using published experimental and numerical results. The effects of wave height, wave frequency, water depth, and PTO damping on the motion response, power generation, and efficiency of the flap WEC are investigated.

2 Numerical Methods

2.1 CFD Theory

The CFD method is used to calculate the numerical change within a finite volume and is based on the theory of viscous hydrodynamics (Isaacson and Cheung 1992, 1991; Mei 2012). The increase in fluid mass is equal to the net mass of the fluid flowing in the microbody. The mass conservation equation, also known as the continuity equation, can be obtained in accordance with this law. The equation is given below:

$$\frac{\partial \rho}{\partial t} + \nabla \cdot (\rho u) = 0 \tag{1}$$

The time averaging method is the most widely used method for studying turbulent fluctuation. The turbulent motion is regarded as the sum of time-averaged flow and pulsating flow.

$$\frac{\partial \rho}{\partial t} + \frac{\partial}{\partial x_i}(\rho u_i) = 0 \tag{2}$$

$$\frac{\partial}{\partial t}(\rho u_i) + \frac{\partial}{\partial x_i}(\rho u_i u_j) = -\frac{\partial p}{\partial x_i} + \frac{\partial}{\partial x_j}\left(\mu \frac{\partial u_i}{\partial x_j} - \rho \overline{u_i' u_j'}\right) + S_i \tag{3}$$

The control equation above shows that an additional item $-\rho \overline{u_i' u_j'}$ exists in the equation. This item is defined as Reynolds Stress and is expressed as $\tau_{ij} = -\rho \overline{u_i' u_j'}$.

The commercial software Star-CCM is used in this work. The fifth order wave theory included in the software is chosen to generate nonlinear waves.

2.2 Wave Energy Absorbing Efficiency

The energy conversion efficiency R of the wave energy conversion device is defined as the ratio of the wave energy E_p captured by the WEC and the incident wave energy E_w per unit time (Henry et al. 2014; Dalton et al. 2010; Kim and Yue 2006). The expression is

$$R = \frac{E_p}{E_w} \tag{4}$$

The mechanical damping coefficient of the energy output system b_{pto} has a great effect on E_p. Thus, when the frequency of the incident wave ω is given, E_p can reach the maximum value when the derivation of the absorption energy rate is 0, $\partial E_p / \partial b_{pto} = 0$. The optimal damping coefficient b_{opt} is

$$b_{pto} = b_{opt} = \sqrt{\frac{\left((I + a_{pto} + a_z)\omega^2 - (c_{pto} + c_z)\right)^2}{\omega^2} + b_z^2} \tag{5}$$

When the moment of inertia and the hydrostatic recovery torque counteract each other, the natural frequency of the flap is the natural frequency. The expression is

$$\omega_n = \sqrt{\frac{c_{pto} + c_z}{I + a_{pto} + a_z}} \tag{6}$$

When the resonance conditions are met such that $\omega_n = \omega$, the mechanical damping coefficient b_{pto} is the same as the radiation damping coefficient b_z. Thus, $b_{pto} = b_z$.

3 Numerical Results and Discussions

3.1 Geometric Parameters of the Device

The case presented by Henry et al. (2014) is carried out for comparison to verify the accuracy of the present model. Flap height is $h = 0.205$ m, and tank depth d is 0.305 m. In this work, the parameters are nondimensionalized with h and d. The thickness and height of the model are 0.0875 m and 0.31 m, respectively. The thickness B, mass m, rotational inertial around the hinge I, and the height of mass center y_c are 0.0875 m, 6.27 kg, 0.1147 kg·m^2, and 0.1324 m, respectively. The width of the two-dimensionl CFD model is set as equal to the thickness of one layer of the grid to reduce the amount of calculation. The mass and rotational inertial should be adjusted in accordance with the ratio of the CFD model width to the real model width.

The damping coefficients are dimensionless as follows (Singh and Sen 2007; Isaacson and Cheung 1991):

$$b_{pto} = \frac{b^*_{pto}}{\rho h^3 g b \sqrt{h/g}} \tag{7}$$

$$c_{pto} = \frac{c^*_{pto}}{\rho h^3 g b} \tag{8}$$

Letters with asterisks represent the dimensional parameter.

3.2 Convergence Study

Generally, wave elevations decay along the wave propagation direction because of fluid viscosity. Therefore, wave generation in the absence of the structure is first calculated to ensure that the generated waves at the position of the structure are the desired waves. The schematic of the computational model is provided in Fig. 1. The following case with wave height $H = 0.1$ m and wave period $T = 1.9$ s is consided. The length of the wave tank is chosen as $L = 4\lambda$ ($\lambda = 3.2$ m). The length of the damping zones at both sides of the computational domain is set as λ. Two different meshes are chosen for the convergence

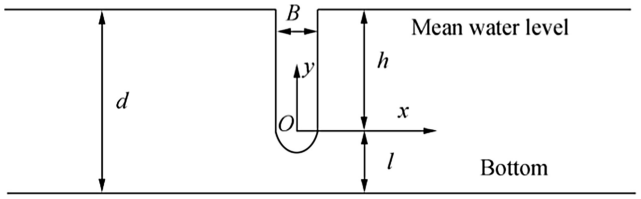

Fig. 1 Schematic of the flap

study. For mesh a, wave height is divided into 20 layers in the vertical direction and wavelengh is divided into 80 parts in the horizontal direction. The element size of mesh b is twice that of mesh a. The time step is set as $\Delta t = T/500$ for both cases. Time step is further subjected to convergence analysis with $\Delta t = T/500$ and $\Delta t = T/1000$ for mesh a. Figure 2 shows the comparisons of wave elevations at the center of the wave tank. The three curves are visually identical and suggests that the simulation with mesh a and $\Delta t = T/500$ is sufficiently accurate. Figure 3 presents the wave height along the wave tank when the wave elevation is stable. The wave height of the whole tank is close to the given wave height. At position $x =$ 3 m, the maximum attenuation of the wave height is approximately 4.2%, which satisfies the demand of accuracy. The above results illustrate that the numerical wave tank can generate stable and accurate waves.

3.3 Verification

The case in Henry et al. (2014) is simulated again for comparison to verify the accuracy of the present model. The time histories of the angular displacement and velocity of the WEC are presented in Fig. 4. The comparison with the experimental and numerical results obtained by Henry et al. (2014) by using Fluent Software is also given. In general, all results are in good agreement. Moreover, the present results, especially the results for the crest value, are close to the experimental data. These results validate the accuracy of the present numerical model.

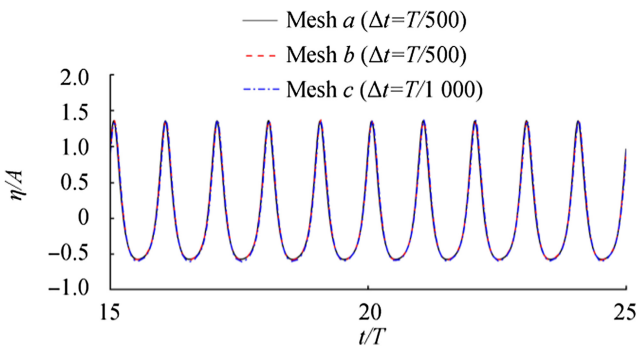

Fig. 2 Convergence study for wave elevations with $H = 0.1$ m at $T = 1.9$ s

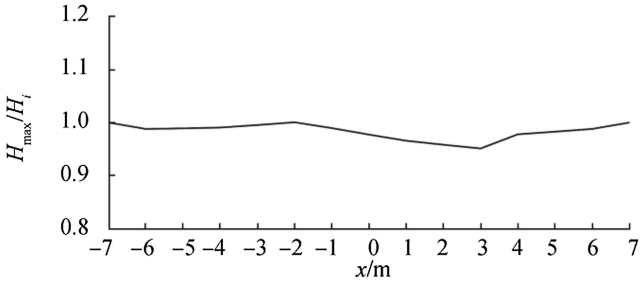

Fig. 3 Wave height attenuation along the propagation direction

3.4 Effect of Design Parameters on the Generator

3.4.1 WEC Performance with Different PTO Damping Coefficients

The maximum wave energy conversion power E_p and conversion efficiency R are obtained when the optimal PTO damping b_{opt} is selected. b_{opt} can be calculated by using Eq. (5) on the basis of the linear frequency domain theory. Different PTO damping coefficients are considered to verify their suitability for the viscous theory and for identifying the effect of PTO damping on motion response. In the experiment discussed in this section, the nondimensional wave height $H = 0.05$, wave frequency $\omega = 0.5$, and water depth $d = 1.4878$ are considered. In this case, the nonlinear effect of small wave height can be neglected. The linear frequency analysis method states that when the wave frequency is 0.5, the added mass of the WEC is $a_z = 0.735$, and the radiation damping is $b_z = 0.339$. The effect of mechanical damping b_{pto} on the energy conversion efficiency when the resonance condition $b_{opt} = b_z$ is satisfied is studied first. Thus, the inertial characteristic a_{pto} and the elastic characteristic c_{pto} of the power output system are set as 0, and $b_{pto} = \upsilon b_{opt}$ is defined. The values of υ are 0.6, 0.8, 1, 1.2, 1.4, and 1.6. The rotation angle, WEC energy absorption, and energy conversion efficiency change with b_{pto} are provided in the following diagram in Fig. 5.

As illustrated in Fig. 5a, the amplitude of the rotation angle gradually decreases as the mechanical damping coefficient b_{pto} increases. Figure 5b and c show that the peak values of the energy absorption and energy conversion efficiency are obtained only when $\upsilon = 1$, but not under the conditions of small damping or large damping. In addition, given that the wave height $H = 0.05$ is in the range of linear theory, when the incident wave frequency equals the natural frequency of the

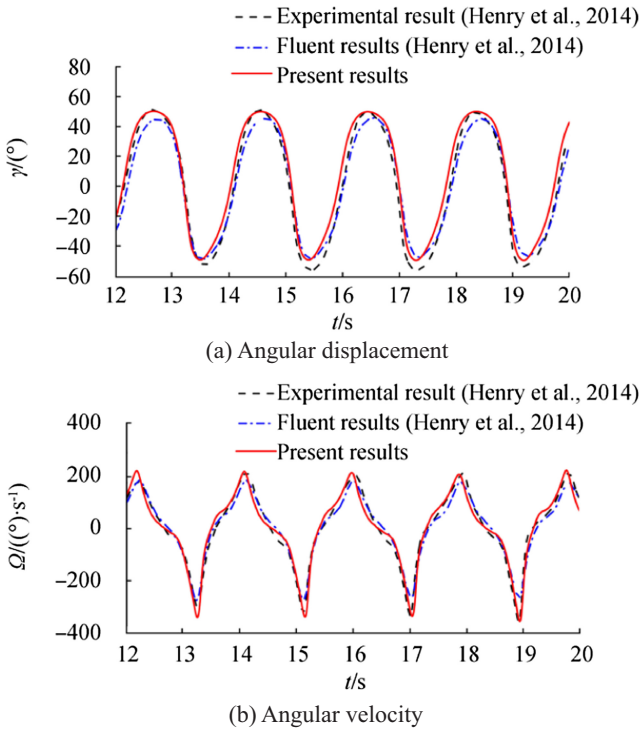

Fig. 4 Comparisons of the angular displacement and velocity results obtained by the present study and those obtained by Henry et al. (2014) through experiments and Fluent simulation

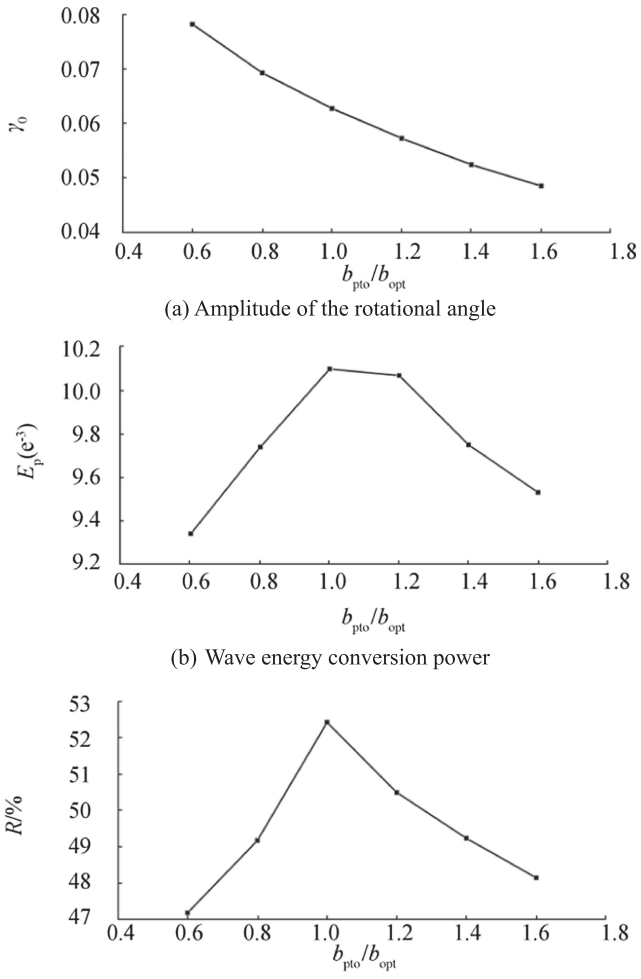

Fig. 5 Variations in γ_0, E_P, and R versus PTO damping coefficients

WEC, and the damping equals the optimal damping b_{opt}, the energy efficiency of the WEC can reach approximately 50%.

3.4.2 WEC Performance at Different Incident Wave Heights

In the experiment presented in this section, we define $a_{pto} = 0$, $b_{pto} = 0.339$, $c_{pto} = 0.091$. As presented in Fig. 6, the trends of the wave energy conversion power E_p and the energy conversion efficiency of the WEC at different wave heights are similar. However, the wave energy conversion power E_p and the energy conversion efficiency of the WEC decrease with increasing wave height because the dissipation of wave energy increases and the energy that could be absorbed by the PTO system decreases. Ning et al. (2016b) similarly regulated the energy absorption E_P and the energy conversion efficiency of the WEC.

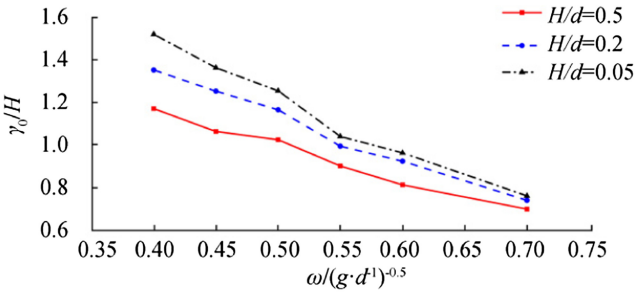

(a) Amplitude of the rotational angle

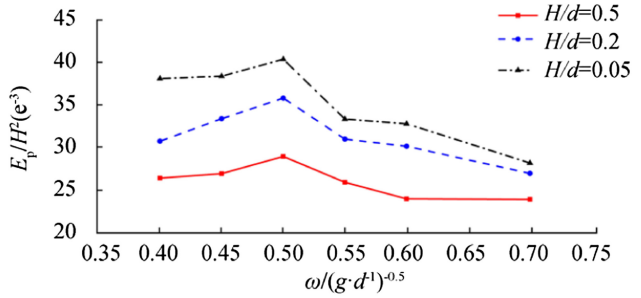

(b) Wave energy conversion power

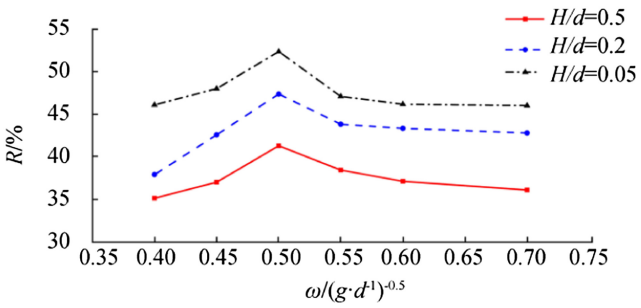

(c) Energy conversion efficiency

Fig. 6 Variations in γ_0, E_P, and R versus nondimensional wave frequeceny at different wave heights and under the optimal PTO damping coefficiencts

3.4.3 WEC Performance at Different Water Depths

For this experiment, we define $a_{pto} = 0$, $b_{pto} = 0.339$, and $c_{pto} = 0.091$. The shallow water effect at different water depths is studied. The Ursell number can be used to explain the shallow water effect and is defined as $Ur = HL^2/d^3$ (Ursell 1953). Here, the maximum Ursell number is $0.0105 \times 3.6^2/0.5^3 \approx 1.08$. The results for the Ursell number indicate that the shallow water effect exists. The variations in the amplitude of of rotational angle, wave energy conversion power of the WEC, and energy conversion efficiency at different water depths are shown in Fig. 7.

Figure 7 shows that water depth has a considerable effect on the amplitude of the rotation angle, the energy conversion power E_p, and the energy conversion efficiency of the WEC. As water depth increases, these three values dramatically decrease. As water depth increases to a critical value, these three parameters remain constant and no longer decrease. This trend is attributed to the shallow water effect. The reciprocal movement of the flap is excited by the wave, and its rotation angle and angular velocity are mainly affected by the horizontal

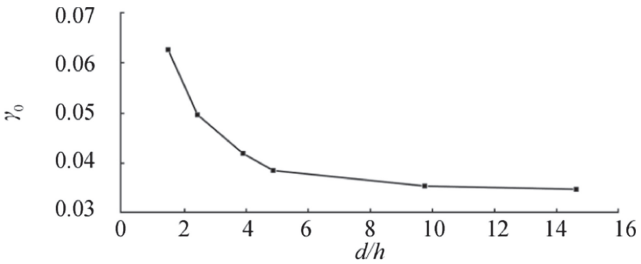

(a) Amplitude of the rotational angle

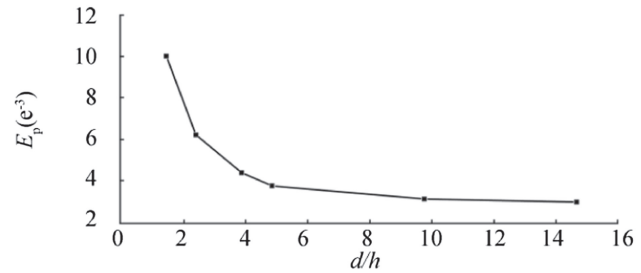

(b) Wave energy conversion power

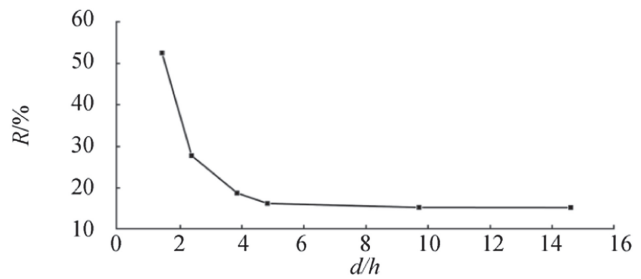

(c) Energy conversion efficiency

Fig. 7 Variations in γ_0, E_P, and R versus water depth

speed of the incident wave. At shallow water depths, the horizontal speed of the incident wave is large, and the exciting force of the flap is large. Thus, the rotation angle and angular velocity of the flap increase, and the power absorption of the WEC will correspondingly increase. Although wave breaking and wave energy dissipation will occur in shallow water, the energy absorption of the WEC in shallow water may not be less than that in deep water. Nevertheless, the impact load of the flap in shallow water will decrease. This effect may prolong the working life of WECs.

4 Conclusions

In this paper, the motion response, wave power, and energy conversion efficiency of a two-dimensional flap-type WEC under the condition of nonlinear regular waves is studied in detail. The following conclusions are obtained:

1) For a given water depth, the nonlinear effect of waves become pronounced, and motion response and energy conversion efficiency decrease as wave height increases.
2) The horizontal speed of water particles in waves, the excitation force of the flap, and the efficiency of the WEC all decrease as water depth increases. The performance of WEC will remain constant and will no longer deteriorate when water depth increases to a critical value.
3) The rotation angle of the WEC decreases rapidly as wave frequency increases. The motion response reduces as the nonlinear effect strengthens. When wave frequency reaches a critical value, the performance of the WEC will remain unchanged as wave frequency increases.

Thus, in the design of oyster WECs, the natural frequency of the WEC should be close to the wave frequency, and the PTO damping should be chosen carefully to increase wave energy conversion efficiency.

Funding This work is supported by the National Natural Science Foundation of China (51409066, 51761135013), the High Technology Ship Scientific Research Project from the Ministry of Industry and Information Technology of the People's Republic of China–Floating Security Platform Project (the second stage, 201622), and the Fundamental Research Fund for the Central University (HEUCFJ180104, HEUCFP1809).

References

Chaplin RV, Aggidis GA (2007) An investigation into power from pitch-surge point-absorber wave energy converters. *International Conference on Clean Electrical Power*. Capri, Italy, 520–525

Chen ZF, Zhou BZ, Zhang L, Li C, Zang J, Zheng XB, Xu JA, Zhang WC (2018a) Experimental and numerical study on a novel dual-resonance wave energy converter with a built-in power take-off system. Energy 165:1008–1020. https://doi.org/10.1016/j.energy.2018.09.094

Chen ZF, Zhou BZ, Zhang L, Sun L, Zhang XW (2018b) Performance evaluation of a dual resonance wave-energy convertor in irregular waves. Appl Ocean Res 77:78–88. https://doi.org/10.1016/j.apor.2018.04.014

Chen ZF, Zhou BZ, Zhang L, Zhang WC, Wang SQ, Zang J (2018c) Geometrical evaluation on the viscous effect of point-absorber wave-energy converters. China Ocean Eng 32(4):443–452. https://doi.org/10.1007/s13344-018-0046-5

Crooks D, Hoff J. van't Folley M, Elsaesser B (2016) Oscillating wave surge converter forced oscillation tests. The 35th International Conference on Ocean, Offshore and Arctic Engineering, Busan, South Korea. https://doi.org/10.1115/omae2016-54660

Dalton GJ, Alcorn R, Lewis T (2010) Case study feasibility analysis of the Pelamis wave energy convertor in Ireland, Portugal and North America. Renew Energy 35(2):443–455. https://doi.org/10.1016/j.renene.2009.07.003

Flocard F, Finnigan TD (2010) Laboratory experiments on the power capture of pitching vertical cylinders in waves. Ocean Eng 37(11):989–997. https://doi.org/10.1016/j.oceaneng.2010.03.011

Folley M, Whittaker T, Vant HJ (2007a) The design of small seabed-mounted bottom-hinged wave energy converters. *The 7th European Wave and Tidal Energy Conference*. Porto, Portugal, 455, 1–10

Folley M, Whittaker TJT, Henry A (2007b) The effect of water depth on the performance of a small surging wave energy converter. Ocean Eng 34(8–9):1265–1274. https://doi.org/10.1016/j.oceaneng.2006.05.015

He F, Huang Z, Law WK (2012) An experimental study of a floating breakwater with asymmetric pneumatic chambers for wave energy extraction. Appl Energy 106(11):222–231. https://doi.org/10.1016/j.apor.2017.06.009

Henry A, Kimmoun O, Nicholson J, Dupont G, Wei Y, Dias F (2014) A two dimensional experimental investigation of slamming of an oscillating wave surge converter. In: Proceedings of the twenty-four International Ocean and Polar Engineering conference, Rusan, Korea

Isaacson M, Cheung KF (1991) Second order wave diffraction around two-dimensional bodies by time-domain method. Appl Ocean Res 13(4):175–186. https://doi.org/10.1016/S0141-1187(05)80073-2

Isaacson M, Cheung KF (1992) Time-domain second-order wave diffraction in three dimensions. J Waterw Port C-ASCE 118(5):496–516. https://doi.org/10.1061/(asce)0733-950x(1992)118:5(496)

Kerr D (2007) Marine energy. Philos T Roy Soc A 365(1853):971–992. https://doi.org/10.1098/rsta.2006.1959

Kim MH, Yue DKP (2006) Complete second-order diffraction solution for an axisymmetric body. Part 2. Bichromatic incident waves and body motions. J Fluid Mech 211:557–593. https://doi.org/10.1017/S0022112090001690

Mei CC (2012) Hydrodynamic principles of wave power extraction. Philos Trans R Soc A Math Phys Eng Sci 370(1959):208–234. https://doi.org/10.1098/rsta.2011.0178

Ning DZ, Zhao XL, Göteman M, Kang H (2016a) Hydrodynamic performance of a pile-restrained WEC-type floating breakwater: an experimental study. Renew Energy 95:531–541. https://doi.org/10.1016/j.renene.2016.04.057

Ning DZ, Wang RQ, Zou QP, Teng B (2016b) An experimental investigation of hydrodynamics of a fixed OWC Wave Energy Converter. Appl Energy 168:636–648. https://doi.org/10.1016/j.apenergy.2016.01.107

Ning DZ, Zhao XL, Hann M, Kang HG (2017) Analytical investigation of hydrodynamic performance of a dual pontoon WEC-type breakwater. Appl Ocean Res 65:102–111. https://doi.org/10.1016/j.apor.2017.03.012

Ogai S, Umeda S, Ishida H (2010) An experimental study of compressed air generation using a pendulum wave energy converter. J Hydrodyn 22(5):290–295. https://doi.org/10.1016/S1001-6058(09)60209-2

Salter SH (1974) Wave power. Nature 249(5459):720–724. https://doi.org/10.1038/249720a0

Singh SP, Sen D (2007) A comparative linear and nonlinear ship motion study using 3-D time domain methods. Ocean Eng 34(13):1863–1881. https://doi.org/10.1016/j.oceaneng.2006.10.016

Sun SY, Sun SL, Wu GX (2018) Fully nonlinear time domain analysis for hydrodynamic performance of an oscillating wave surge converter. China Ocean Eng 32(5):582–592. https://doi.org/10.1007/s13344-018-0060-7

Ursell F (1953) The long-wave paradox in the theory of gravity waves. Math Proc Camb Philos Soc 49(4):685. https://doi.org/10.1017/s0305004100028887

Wei Y, Rafiee A, Henry A, Dias F (2015) Wave interaction with an oscillating wave surge *converter*, part I: viscous effects. Ocean Eng 104:185–203. https://doi.org/10.1016/j.oceaneng.2015.05.002

Wei Y, Abadie T, Henry A, Dias F (2016) Wave interaction with an oscillating wave surge converter. Part II: slamming. Ocean Eng 113:319–334. https://doi.org/10.1016/j.oceaneng.2015.12.041

Zhao H, Sun Z, Hao C, Shen J (2013) Numerical modeling on hydrodynamic performance of a bottom-hinged flap wave energy converter. China Ocean Eng 27(1):73–86. https://doi.org/10.1007/s13344-013-0007-y